

Large-area interdigitated array microelectrodes for electrochemical sensing

Adam E. Cohen¹, Roderick R. Kunz^{*}

Lincoln Laboratory, Massachusetts Institute of Technology, 244 Wood Street, Mailstop C-171, Lexington, MA 0242-9108, USA

Received 8 February 1999; received in revised form 27 July 1999; accepted 27 July 1999

Abstract

Advanced photolithography developed for the semiconductor industry has been used to fabricate interdigitated microelectrode arrays that pass steady-state limiting currents of up to 230 nA/ μM analyte — 2.5 times more than the most sensitive interdigitated array built to date, and exhibit response times of ~ 5 ms. This performance results from the small interelectrode gap and the large active area of the device (4 mm²), a combination enabled by advanced photolithography. We describe the fabrication of these arrays and the characterization of their performance in two environments: an aqueous solution of $\text{Ru}(\text{NH}_3)_6^{3+}$ and a dinitrotoluene solution in acetonitrile. The scaling of array performance parameters with device dimensions is also presented. © 2000 Elsevier Science S.A. All rights reserved.

Keywords: Interdigitated array microelectrodes; Electrochemical sensing; Photolithography

1. Introduction

Various microelectrode geometries have been evaluated in recent years in attempts to increase their detection sensitivity by minimizing the effects of analyte depletion and double-layer charging current during the measurement of reversible redox species. One geometry that has drawn particular interest is that of interdigitated arrays of microelectrodes. In the interdigitated array (IDA) configuration, one electrode is held at a potential to drive the reduction $O + ne \rightarrow R$, while the other electrode is held at a potential to drive the oxidation $R \rightarrow O + ne$. Species produced at one electrode diffuse to the other electrode, where they are converted back to their original form, creating a process called redox cycling. This cycling between the two electrodes can lead to a greatly amplified current (Fig. 1), and was first demonstrated by Bard et al. [1] in 1986 using two photolithographically patterned microelectrodes, the generator and collector electrodes. Decreasing the dimensions of the electrodes and the interelectrode gap increases the cycling efficiency, because fewer ions diffuse back into the

bulk solution. The signal enhancements derived from such IDAs have been used for detection of electroactive compounds such as dopamine and catecholamine [1–10]. The arrays also have potential for more exotic uses such as diffraction-based photoelectrochemical detection, studies of diffusion [11], and measurements of reaction kinetics [1,5,7]. Quantitative analyses of IDAs have also been developed [1,12,13], and electrodes spaced as closely as 800 nm have been fabricated [13]. For most of these scaled devices, redox cycling efficiencies (i.e., faradaic current enhancements) on the order of 40 have been reported. The only example of redox cycling using deep submicrometer interelectrode gaps was achieved with a modified atomic force microscope tip [14], where faradaic currents corresponding to redox species' cycling frequencies in excess of $\sim 10^6$ Hz were reported for an interelectrode gap of 15 nm. This sensing method, however, is not practical for many applications due to the very small electrode area. Furthermore, no systematic study has been performed to date on the effects of intermediate values of electrode spacing on sensitivity and response time. This paper is, to our knowledge, the first report on the fabrication of scaled IDAs using state-of-the-art yet practical lithographies. We also report on the performance of these sensors which have a sensitivity higher than any other IDAs, and analyze the advantages enabled by lithographic scaling. In fact, a

^{*} Corresponding author. Tel.: +1-781-981-7812; e-mail: kunz@11.mit.edu

¹ Current address: 170 Winthrop Mail Center, Cambridge, MA 02138.

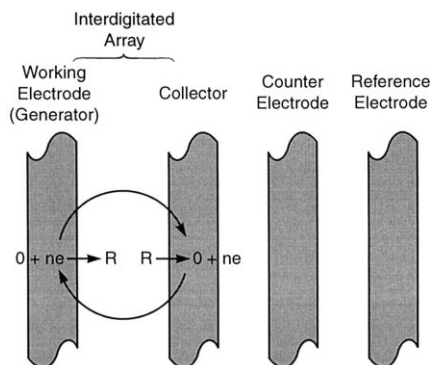


Fig. 1. Redox cycling in an interdigitated array. The setup can be run as a standard three-electrode cell (working, counter, reference) or in redox cycling mode using four electrodes by “turning on” the collector to prevent depletion of O near the work electrode.

straightforward extension of the fabrication method used in our experiments has the potential to generate practical IDAs with a sensitivity of < 1 ppb of analyte at response times in the millisecond range. This would represent a performance regime not yet realized in IDA sensors.

2. Materials and methods

2.1. Sensor fabrication

Five sensors have been fabricated, each sensor consisting of an interdigitated electrode array shown in Fig. 2. The finger length b is 2 mm in all arrays. The electrode width w_f is varied from 0.5 to 5 μm , and the electrode gap w_g is varied from 0.15 to 5 μm . Each array has an active area of 2 mm^2 . The patterning process is illustrated in Fig. 3. A deep-ultraviolet exposure tool operating at 193 nm replicated the sensor pattern. The resist used was a poly(vinyl phenol) resin which acts as a top-surface imaged dry-developed resist [15], which allowed control over the developed resist profiles to obtain slight overhangs, thereby facilitating the subsequent metal liftoff step. Following photoresist patterning, a platinum liftoff was performed. Fig. 4(a) shows an electron micrograph of re-en-

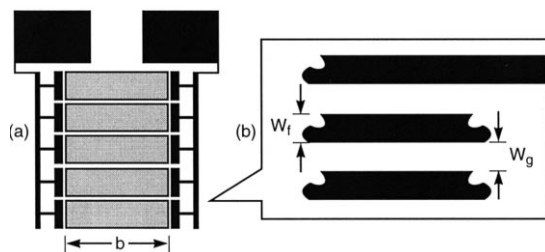


Fig. 2. Layout of the interdigitated sensor: (a) macroscopic configuration with the contact pads on top. (b) microscopic configuration. b is the finger length, w_f is the electrode width, w_g is the interelectrode gap, and m (not shown) is the number of pairs of fingers.

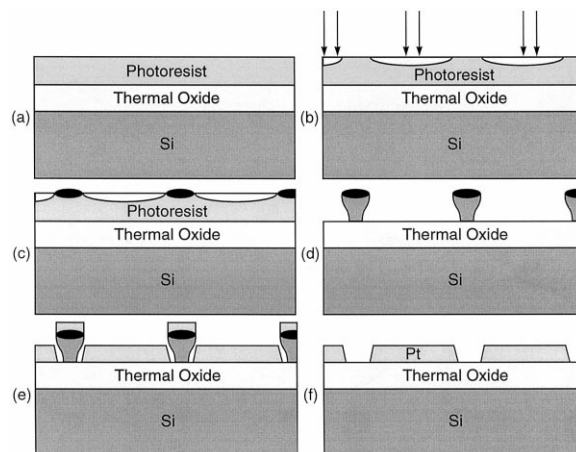


Fig. 3. (a) Thermal growth of 500 nm oxide on a silicon wafer, followed by coating of the oxide with poly(vinyl phenol), which acts as a dry-developed resist; (b) exposure in a 193-nm, 0.5-NA projection system; (c) silylation using dimethylsilyldimethylamine; (d) dry development to generate reentrant profile; (e) evaporation of 100 nm Pt onto the wafer; (f) removal of the remaining photoresist by sonication for 1 h in EKC 265 resist stripper at 55°C, leaving the desired pattern on the wafer.

trant resist profile created using this process and Fig. 4(b) shows a completed sensor.

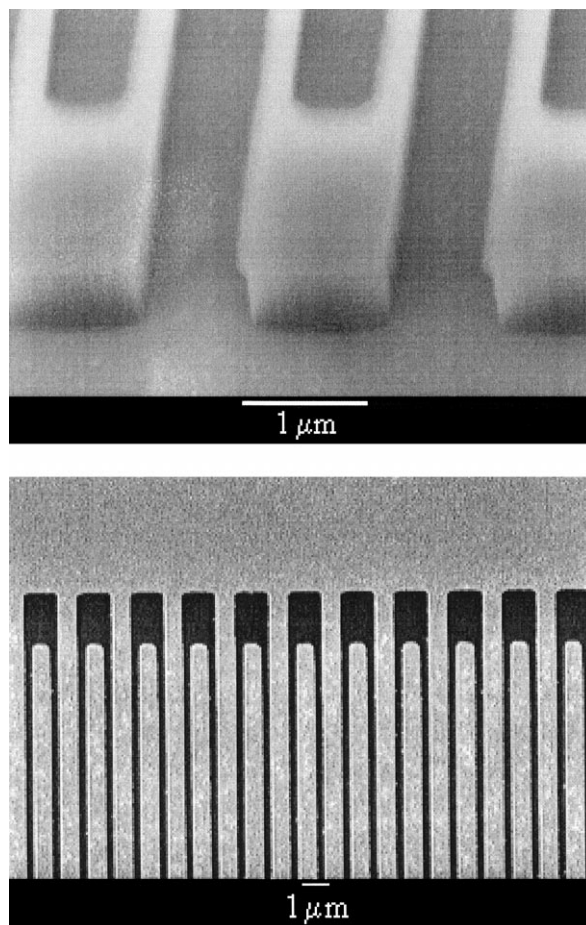


Fig. 4. Electron micrographs of (a) reentrant resist profile and (b) completed sensor (array B in Table 1).

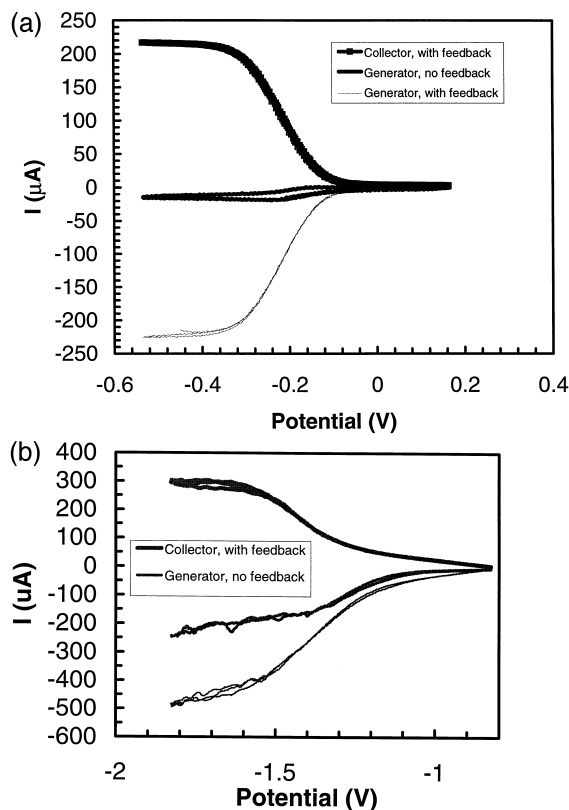


Fig. 5. (a) Redox cycling in array **D** (see Table 1) in 1 mM $\text{Ru}(\text{NH}_3)_6^{3+}$ in 0.1 M KCl; sweep rate = 50 mV/s; with feedback, collector potential = 0.1 V vs. Ag/AgCl. (b) Redox cycling in array **B** (Table 1) electrode in 1mM dinitrotoluene (DNT) in 0.2 M tetrabutylammonium perchlorate in acetonitrile; sweep rate = 50 mV/s; with feedback, collector potential = -0.8 V vs. Ag/AgNO₃.

2.2. Chemicals and hardware

The redox cycling ability of the arrays was tested in an aqueous solution of $\text{Ru}(\text{NH}_3)_6^{3+}$ (Strem Chemicals) in 0.1-M $\text{KCl}_{(\text{aq})}$, and in dinitrotoluene (Aldrich) in 0.2-M tetrabutylammonium perchlorate (Sigma) in acetonitrile (Sigma). All reagents were used as received. Cyclic voltammograms were recorded on a Princeton Applied Research Model 173 Potentiostat/Galvanostat with a home-built second potentiostat channel [16]. In aqueous solution, voltages were measured and are reported with

respect to an Ag/AgCl reference electrode (Bioanalytical Systems), and in acetonitrile, voltages were measured and are reported with respect to an Ag/AgNO₃ organic electrochemistry reference electrode (Bioanalytical Systems). Data from the potentiostat were digitized and recorded on a personal computer.

In a typical experiment, a chip was mounted on a Teflon board and electrical contacts were made via ‘‘alligator’’ clips attached to the contact pads. The chip was rinsed in deionized water and dried under a stream of nitrogen. The electrolyte solution was used as prepared. The chip was immersed in the solution to completely wet the array surface while leaving the contact pads dry. The surface area of the metal buses connecting the array to the contact pads was approximately 10% of the total array area. While species reacting on these metal buses did not undergo redox cycling, the total uncertainty introduced by this effect is expected to be small.

3. Data and analysis

3.1. Experimental results

We first measured the redox current for an aqueous solution of $\text{Ru}(\text{NH}_3)_6^{3+}$ in a conventional three electrode arrangement (Fig. 5a, generator, no feedback) and compared it to the current with a potential applied to the fourth, collector electrode (Fig. 5a, generator, with feedback). Our results demonstrate that the faradaic signal is significantly enhanced when the array performs redox cycling. Table 1 shows the performance characteristics of all five arrays in the $\text{Ru}(\text{NH}_3)_6^{3+}$ solution. The **C** electrodes give a signal of 232 nA/μM analyte, while the **A** electrodes pass 176 nA/μM analyte (Table 1). Fig. 6 shows the redox cycling current for $\text{Ru}(\text{NH}_3)_6^{3+}$ solutions all four arrays tests vs. a geometric parameter Φ (to be discussed later). This parameter, which has units of distance, describes the proximity of the generator and collector electrodes. The current in the **A** array reaches its steady-state value within 5 msec after the feedback is turned on. An **A** electrode operated continuously in solution with little change in current for almost one and a half

Table 1

Performance of the five arrays in 1 mM $\text{Ru}(\text{NH}_3)_6^{3+}$ in 0.1 M KCl. The array characteristics are w_g (interelectrode gap), w_f (finger width), b (finger length), and m (number of pairs of fingers). To measure I_{lim} without feedback, the potential was swept at 5 mV/s. The gain is calculated by dividing the limiting current with feedback by the limiting current without feedback. See text for a discussion of Φ

Array	w_g (μm)	w_f (μm)	b (mm)	m	I_{lim} (μA), no feedback	I_{lim} (μA), collector at +0.1 V	Gain	Φ (m)
L	5	5	2	100	4.8	17.5	3.6	0.20
A	0.5	0.5	2	1000	4.5	176	39	2.0
B	0.25	0.75	2	1000	4.5	218	48	2.9
C	0.2	0.80	2	1000	4.8	232	48	3.2
D	0.15	0.85	2	1000	6.4	220	34	3.6

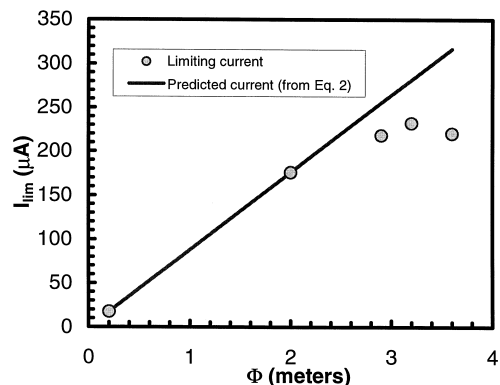


Fig. 6. Limiting current as a function of the geometric parameter Φ . The drop in current below the predicted value for large values of Φ is probably the result of defects in arrays with very small geometries, although other possible explanations have not been ruled out.

hours (Fig. 7). In addition we used non-aqueous solutions of dinitrotoluene and observed signals of $500 \text{ nA}/\mu\text{M}$ (Fig. 5b). However, this represents only a $2 \times$ gain over the three-electrode configuration compared to the $40\text{--}50 \times$ enhancements we saw in the aqueous $\text{Ru}(\text{NH}_3)_6^{3+}$ solutions.

Aoki et al. [2] previously developed a quantitative prediction for the current that should flow in an IDA operating in redox cycling mode:

$$|I_{\text{lim}}| = nFDC^*mb \left[0.637 \ln \left(2.55 \left(1 + \frac{w_f}{w_g} \right) \right) - \frac{0.19}{\left(1 + \frac{w_f}{w_g} \right)^2} \right] \quad (1)$$

where $|I_{\text{lim}}|$ is the absolute value of the steady-state current, nF is the charge transferred per mole of analyte reacted, D is the analyte's diffusion coefficient, C^* is the

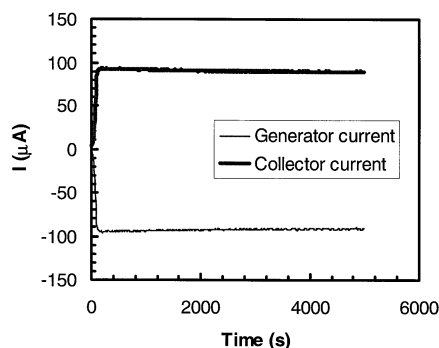


Fig. 7. Redox cycling on an A electrode in $0.4 \text{ mM Ru}(\text{NH}_3)_6^{3+}$ in 0.1 M KCl , showing the long-term stability of the redox cycling current. The magnitude of the generator current falls slightly over time as irreversible side reactions slowly deplete reagent and/or poison the electrode surface, while the collector current remains essentially constant.

bulk analyte concentration, m is the number of pairs of “fingers” in the array, b is the length of each finger, w_f is the electrode width, and w_g is the interelectrode gap. The terms containing m , b , w_f , and w_g collectively describe the array geometry and represent the value Φ used in Fig. 6. The derivation of this equation assumes that the potentials on the electrodes are such that the reaction rate is mass transport limited; that the analyte moves only via diffusion; that the widths of the generator and collector electrodes are equal; and that D is constant for both the oxidized and reduced species, and it is constant everywhere in the solution. All these assumptions apply in our experimental setup.

The limiting current for the B, C and D electrodes in $\text{Ru}(\text{NH}_3)_6^{3+}$ solution is lower than that predicted by the equation of Aoki et al. [2] by 15, 19 and 31%, respectively. We tentatively attribute this deviation to possible defects on the arrays tested, which prevent redox cycling from occurring in some sections of the arrays. Our electrical inspection of the arrays revealed consistently high values of interelectrode resistance ($> 0.1 \text{ M}\Omega$) for the L and A arrays (it was not infinite due to residual surface conductivity of the SiO_2 substrate). However, we found interelectrode resistance values to vary from array to array for the B, C, and D arrays. Although our lithographic techniques are easily capable of yielding defect-free devices of this size and geometry, we know that the platinum lift-off step is prone to producing metallic particles which can cause electrical shorts. Due to the relatively high resistance of the electrode fingers themselves ($\sim 1 \text{ k}\Omega$), however, a single short circuit might not render an entire array inoperable. Some fingers in the arrays may also have been disconnected from the voltage supply. However, other reasons for the deviation of experimental results from the predicted linear behavior (Fig. 6) have not been ruled out.

As predicted by Aoki et al. [2], the current is linear in the analyte concentration (Fig. 8). A C array in a neat KCl

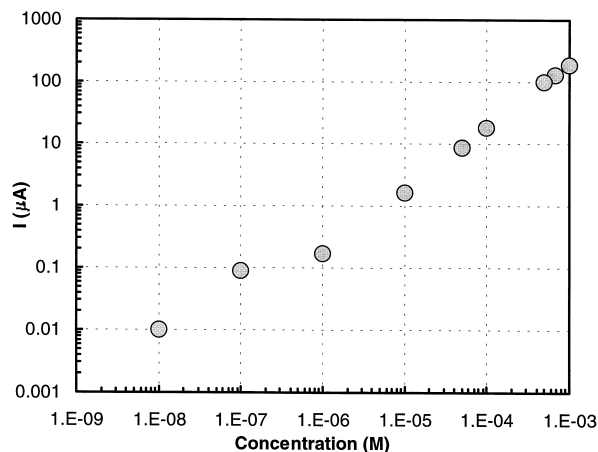


Fig. 8. Cycling current as a function of the concentration of $\text{Ru}(\text{NH}_3)_6^{3+}$ in 0.1 M KCl at an A electrode. The slope corresponds to a sensitivity of $180 \text{ nA}/\mu\text{M}$.

electrolyte solution passes a current of approximately 10 nA. Requiring the redox cycling signal to be at least twice the signal level from neat solution gives the C electrode a detection threshold of 86 nM, or approximately 2 ppb. From our data, we see that the current per finger is independent of the electrode width and interelectrode gap, provided that the ratio of the two remains constant, and the difference in current between the L array and the A array is solely due to the difference in the number of fingers between the two arrays.

3.2. Scaling of electrode dimensions in redox cycling experiments

The results in the previous section experimentally demonstrate how scaling enhances performance. Understanding how this behavior changes with further scaling or rearrangement of the system's geometry should allow the design of further improved electrode configurations. The performance characteristics of interest in an interdigitated microelectrode array are (1) the attainable limiting current under redox cycling I_{lim} , (2) the device's temporal response to a change in analyte concentration or in the voltage applied to one or both electrodes, and (3) the effect of an irreversible component to the reaction. We treat these topics to varying degrees of rigor, assuming that mass transport occurs only through diffusion, the reaction rate is limited by mass transport, and the diffusion coefficient is constant for both the oxidized and reduced species and at all locations in the solution. Certain experimental conditions, such as stirring the solution, may give different results from those predicted here.

3.2.1. Limiting current

For most applications a large enhancement in the limiting current is the desired result of a novel redox cycling electrode design. We describe a technique that greatly simplifies the first-order calculation of the limiting current for many electrode configurations, provided the current is limited by interelectrode mass transport. To do this, let

$$I_{\text{lim}} = nFDC^*\Phi \quad (2)$$

where Φ is substituted for the complex geometric term in Eq. (1). This parameter Φ has the units of length and as described earlier, is the geometric term describing the proximity of the generator and collector electrodes. IDAs with the greatest value of Φ will exhibit the greatest limiting currents. A simplified way to analytically determine optimized Φ values can be made with assistance of an assumption outlined in Appendix A. This assumption describes that, for the ideal case where the interelectrode analyte mass transport is diffusion limited, the faradaic current in an electrochemical cell is analogous to the ohmic current between two electrodes submersed in a medium of constant resistivity R , yielding an analogous expression for ohmic current flow:

$$I = \sigma V\Phi \quad (3)$$

where σ is the medium's conductivity. Given this, one can then use the well-developed models for electrostatics to determine an electrode geometry that gives the highest effective value for Φ . This might suggest non-planar electrode configurations (e.g., arrays of "point" electrodes) or other geometries not considered previously.

Experimentally, a quantitative comparison of Φ can be arrived by calculation of I_{lim}/C^* , the normalized limiting current. Our value of 232 nA/ μM is $2.5 \times$ higher than the highest previously reported value. Direct calculation of Φ from Eq. (1) yields 3.6 m, which also yields a factor $\sim 2.5 \times$ higher than the highest previous value of 1.49 m.

However, there are cases, particularly at very small electrode gaps, where the limiting current is governed by reaction kinetics rather than mass transport. For these cases, such a simple expression as Eq. (3) does not apply, but rather the current can be calculated assuming Butler-Volmer [17] kinetics. A more rigorous derivation [18] for the limiting current as a function of interelectrode spacing has been derived that predicts the transition from diffusion-limited to kinetics-limited redox cycling, but the derivation is beyond the scope of this paper.

3.2.2. Temporal response

Two characteristic times govern the temporal response of a redox cycling electrode configuration: the time constant for the capacitive charging of the double layer, and the mean time for an analyte molecule to diffuse from the generator to the collector.

The capacitive time constant comes into effect when the voltage on one of the electrodes is changing. The time constant for double-layer charging is RC , where R is the solution resistance measured between the generator and collector electrodes and C is the double-layer capacitance of one electrode. The solution resistance R is inversely proportional to the limiting current I_{lim} , and for certain microelectrode designs the resistance of the electrodes may be a significant factor as well. Meanwhile, the capacitance of an electrode's double layer is directly proportional to the electrode's surface area. An electrode design seeking to minimize the time constant for the charging current should maximize Φ , while keeping the electrode surface area to a minimum — a condition only achieved in small arrays of aggressively scaled electrodes.

The analyte transit time between the generator and collector affects sensor performance either when the analyte concentration is changing rapidly or when the sensor is switched between a redox cycling and noncycling mode. The mean time τ for a species to diffuse from the generator to the collector is given by

$$\tau = \frac{\Delta^2}{2D} \quad (4)$$

where Δ is the mean distance between the two electrodes. The precise calculation of Δ can be quite complicated.

Nonetheless, it is a useful measure because Δ scales linearly with the size of the sensor along the direction of diffusion. In many configurations the direction of diffusion is obvious from considerations of the symmetry of the electrode array. A typical diffusion coefficient for a small molecule in solution is $5 \times 10^{-6} \text{ cm}^2/\text{s}$, so an interdigitated array with $\Delta = 1 \text{ }\mu\text{m}$ will respond in approximately 1 ms. Depending on the application, a large or small transit time may be required. It is important to note that τ and Φ can vary independently of each other. For example, in the case of two closely spaced parallel plate electrodes, increasing the surface area of the electrodes will increase Φ , but not τ .

3.2.3. Analyte irreversibility

Two types of side reactions can render an analyte molecule unavailable for subsequent redox cycling. A reaction may occur in the solution, in which case decreasing the interelectrode gap will increase the probability that the molecule reaches an electrode where it can be cycled, before the reaction occurs. Thus, decreasing the interelectrode gap to minimize the device response time will also increase the limiting current for redox systems with unstable intermediates. A similar effect was shown many years ago for the rotating ring-disc electrode. A side reaction may also occur on the electrode surface, in which case the electrode geometry will have no impact on the probability that the side reaction occurs, and the only way to maximize the limiting current will be to maximize Φ . By investigating the effect of the interelectrode gap on the limiting current, it should be possible to gain insight into the mechanisms of side reactions.

4. Conclusion

We have demonstrated that high-resolution photolithography can be used to fabricate electrochemical sensors with greatly improved performance. Our experiments partially close the gap between the dimensions attained in proximal probe electrochemistry experiments [14,19] and those achieved by conventional photolithography. The benefit of smaller electrode geometries can now be practically realized simply from the fact that with smaller electrodes, more of them can be photolithographically patterned into a fixed area. In fact, using the same exposure tool used to fabricate these $(2 \text{ mm})^2$ arrays, devices whose overall area was $(20 \text{ mm})^2$ would have been just as easy to fabricate, further increasing the signal by another factor of 100 (with probably a somewhat lesser increase in noise as well). Even though the resultant arrays would now have occupied 400 mm^2 , such a mass-produced device whose sensitivity was on the order of $\sim 25 \text{ nA/nM}$ (i.e., 25 nA at a concentration of $\sim 20 \text{ ppt}$) and with a response time of tens of milliseconds, could offer utility for certain monitoring applications such as liquid chromatography [6,8,9],

meso- and micro-scale fluidics, and process monitoring. In addition, our detection of dinitrotoluene suggests that IDAs can be used to detect other nitroaromatic compounds used in explosives, possibly in applications such as ground water contamination.

We also propose an intuitive physical analogy to redox cycling systems which can be applied to design microelectrodes with optimum redox cycling characteristics. Based on these estimates, we expect that detectors capable of $\ll 1 \text{ ppb}$ detection limits whose response times are on the order of milliseconds, or less-sensitive ultrafast electrodes whose response times are $< 1 \text{ ms}$ can be inexpensively mass produced via modern photolithographic techniques. While anodic stripping voltammetry can achieve similar sensitivities, it requires a preconcentration period on the order of 10 min prior to the measurement [20]. Thus, our IDAs give an unprecedented combination of speed and sensitivity.

Acknowledgements

We thank Scott Doran for help in the fabrication of the interdigitated arrays used in this study and Karen Challenge for help in the preparation of this manuscript. This work was sponsored by the United States Air Force under Air Force Contract F19628-95-C-002. Opinions, interpretations, conclusions, and recommendations are those of the authors, and do not necessarily represent the view of the United States Air Force.

Appendix A

Proof that interelectrode geometry affects the faradaic-limiting and ohmic currents in a similar fashion, i.e.,

$$I_{\text{lim}} = nFDC^*\Phi \sim \sigma V\Phi \quad (\text{A.1})$$

where Φ is dependent only on the geometry between the two electrodes.

To begin, take the reaction $\text{O} + ne \leftrightarrow \text{R}$, undergoing redox cycling under steady-state conditions. The following boundary conditions apply: far from the electrodes $[C_{\text{O}}] = C^*$ and $[C_{\text{R}}] = 0$; on the generator electrode surface $[C_{\text{O}}] = 0$ and $[C_{\text{R}}] = C^*$; and on the collector electrode surface $[C_{\text{O}}] = C^*$ and $[C_{\text{R}}] = 0$.

By definition of steady-state conditions, $[C_{\text{O}}]$ at any point in the solution is constant with time, and $[C_{\text{R}}]$ at any point in the solution is constant with time. Fick's second law of diffusion then states that

$$\nabla^2[C_{\text{O}}] = 0 \quad \nabla^2[C_{\text{R}}] = 0 \quad (\text{A.2})$$

everywhere except on the electrode surfaces, where the boundary conditions apply. The Helmholtz theorem [21] tells us that this is enough information to uniquely specify $[C_{\text{O}}]$ and $[C_{\text{R}}]$ everywhere in the solution.

Now let us consider the hypothetical resistive case. Here the potential at the generator is V_0 , and the potential at the collector is 0, as is the potential at infinity. Everywhere in the medium

$$\nabla^2 V = 0 \quad (\text{A.3})$$

if there is to be no buildup of charge. Thus the bulk equations for V and $[C_R]$ are the same, and the boundary conditions for V and $[C_R]$ are directly proportional to each other. Using the Helmholtz theorem and the linearity of the Laplacian, we can then conclude that everywhere in the solution.

$$\frac{V}{V_0} = \frac{[C_R]}{C^*} \quad (\text{A.4})$$

The limiting current at the collector is provided by the diffusion of C_R :

$$I_{\text{lim}} = nFD\phi \nabla [C_R] d\vec{a} \quad (\text{A.5})$$

where the integral is taken over some closed surface around the collector electrode. Similarly, the electric current in the resistive case is given by

$$I_{\text{hyp}} = \sigma \phi \nabla V d\vec{a} \quad (\text{A.6})$$

integrated over the same boundary. Since

$$\nabla [C_R] = \frac{C^*}{V_0} \nabla V \quad (\text{A.7})$$

we can substitute Eq. (A.6) and Eq. (A.7) into Eq. (A.5) to yield our result:

$$I_{\text{lim}} = nFDC^* \frac{I_{\text{hyp}}}{\sigma V_0}, \quad (\text{A.8})$$

Or simply,

$$nFDC^* = \sigma V_0 \quad (\text{A.9})$$

and hence

$$I_{\text{lim}} = nFDC^* \Phi = \sigma V_0 \Phi \quad (\text{A.10})$$

A parallel argument applied to the generator electrode yields the same result.

References

- [1] A.J. Bard, J.A. Crayston, G.P. Kittlesen, T. Varco Shea, M.S. Wrighton, Digital simulation of the measured electrochemical response of reversible redox couples at microelectrode arrays: consequences arising from closely spaced ultramicroelectrodes, *Anal. Chem.* 58 (1986) 2321–2331.
- [2] K. Aoki, M. Morita, O. Niwa, H. Tabei, Quantitative analysis of reversible diffusion-controlled currents of redox soluble species at interdigitated array electrodes under steady-state conditions, *J. Electroanal. Chem.* 256 (1988) 269–282.
- [3] O. Niwa, M. Morita, H. Tabei, Electrochemical behavior of reversible redox species at interdigitated array electrodes with different geometries: consideration of redox cycling and collection efficiency, *Anal. Chem.* 62 (1990) 447–452.
- [4] M. Paeschke, U. Wollenberger, T. Lisec, U. Schnakenberg, R. Hintsche, Highly sensitive electrochemical microsensors using sub-micrometer electrode arrays, *Sens. Actuators, B* 26–27 (1995) 394–397.
- [5] U. Wollenberger, M. Paeschke, R. Hintsche, Interdigitated array microelectrodes for the determination of enzyme activities, *Analyst* 119 (1994) 1245–1249.
- [6] O. Niwa, M. Morita, H. Tabei, Highly sensitive small volume voltammetry of reversible redox species with an IDA electrochemical cell and its application to selective detection of catecholamine, *Sens. Actuators, B* 13–14 (1993) 558–560.
- [7] K. Reimer, C. Kohler, T. Lisec, U. Schnakenberg, G. Fuhr, R. Hintsche, B. Wagner, Fabrication of electrode arrays in the quarter micron regime for biotechnological applications, *Sens. Actuators, A* 46–47 (1995) 66–70.
- [8] O. Niwa, M. Morita, H. Tabei, Highly selective electrochemical detection of dopamine using interdigitated array electrodes modified with Nafion/polyester ionomer layered film, *Electroanalysis* 6 (1994) 237–243.
- [9] M. Takahashi, M. Morita, O. Niwa, H. Tabei, Highly sensitive high-performance liquid chromatography detection of catecholamine with interdigitated array microelectrodes, *J. Electroanal. Chem.* 335 (1992) 253–263.
- [10] M. Takahashi, M. Morita, O. Niwa, H. Tabei, Highly sensitive detection of catecholamine with interdigitated array microelectrodes in HPLC, *Sens. Actuators, B* 13–14 (1993) 336–339.
- [11] C. Chen, T.A. Postlethwaite, J.E. Hutchinson, E.T. Samulski, R.W. Murray, Electrochemical measurements of anisotropic diffusion in thin lyotropic liquid crystal films, *Electroanalysis* 6 (1994) 237–243.
- [12] B. Fosset, C.A. Amatore, J.E. Bartelt, R.M. Wightman, Theory and experiment for the collector-generator triple-band electrode, *Anal. Chem.* 63 (1991) 1403–1408.
- [13] B. Fosset, C.A. Amatore, J.E. Bartelt, A.C. Michael, R.M. Wightman, Use of conformal maps to model the voltammetric response of collector-generator double-band electrodes, *Anal. Chem.* 63 (1991) 306–314.
- [14] F.F. Fan, J. Kwak, A.J. Bard, Single molecule electrochemistry, *J. Am. Chem. Soc.* 118 (1996) 9669–9675.
- [15] S.C. Palmateer, R.R. Kunz, M.W. Horn, A.R. Forte, M. Rothschild, Optimization of a 193-nm silylation process for sub-0.25- μm lithography, *SPIE Proc.* 2438 (1995) 455–464.
- [16] A.J. Bard, L. Faulkner, *Electrochemical Methods: Fundamentals and Applications*, Wiley, New York, 1980, pp. 566–567.
- [17] *ibid.* pp. 91–96.
- [18] A.E. Cohen, R.R. Kunz, in preparation.
- [19] F.F. Fan, A.J. Bard, Electrochemical detection of single molecules, *Science* 267 (1995) 871–874.
- [20] G.T.A. Kovacs, C.W. Stormont, S.P. Kounaves, Microfabricated heavy metal ion sensor, *Sens. Actuators, B* 23 (1995) 41–47.
- [21] David J. Griffiths, *Introduction to Electrodynamics*, 2nd edn., Prentice Hall, Englewood Cliffs, NJ, 1989, pp. 54–56, 270–276.